

Facility for Heavy-Ion Irradiation of Semiconductors at RIKEN RI-Beam Factory

T. Kambara and A. Yoshida, *RIKEN Nishina Center*

Published in 2018 IEEE Radiation Effects Data Workshop (REDW) Workshop Record
 DOI: 10.1109/NSREC.2018.8584278
 Publisher: IEEE
<https://ieeexplore.ieee.org/document/8584278>

Abstract-- RIKEN RI-Beam Factory (RIBF) provides fast Kr and Ar ions to private companies in Japan for the SEE evaluations of space-use semiconductors. The samples can be irradiated in the atmosphere. We present the irradiation facility and measurements of the beam characteristics and discuss radiochemical analyses and simulations concerning the beam impurity nuclides produced in the upstream materials.

I. INTRODUCTION

RI Beam Factory (RIBF) of RIKEN Nishina Center (RNC) [1] is a heavy-ion accelerator facility located near Tokyo, Japan. RIBF features high intensity beams of ions of all elements with energy up to 345 MeV/u and various radioactive isotope beams (RI beams) produced by fragment separators. The beams from RIBF are mainly used for experiments of nuclear physics, materials sciences, chemistry, and radiation biology. In 2014, RNC started to provide fast heavy ions from the RIKEN Ring Cyclotron (RRC) housed in RIBF to private companies in Japan which evaluate single-event effects (SEEs) of space-use semiconductors. In section 2, we present the ion beams and irradiation facility for semiconductor irradiation. In section 3, we describe the procedures and results of the beam characteristics measurements. Then we discuss beam-impurity nuclides produced in the upstream materials; radiochemical measurements of their production probabilities in section 4 and ion-transport simulations in section 5.

II. BEAM AND FACILITY

The RRC with an AVF cyclotron as injector sends a heavy-ion beam to a beam line dedicated to material irradiations. At present, beams of 95 MeV/u Ar and 70

MeV/u Kr ions are in practical use while beams of Xe and Au ions are being tested. The clients irradiate their samples in the atmosphere, which enables easy access and quick exchange of the samples without vacuum feedthrough flanges for electrical connections. With a beam-energy degrader, the clients can select linear energy transfer (LET) in Si between 2.2 and 41 MeV/(mg/cm²). Fig. 1 shows the relation between the LET and range in Si for beams available at RIBF and other facilities.

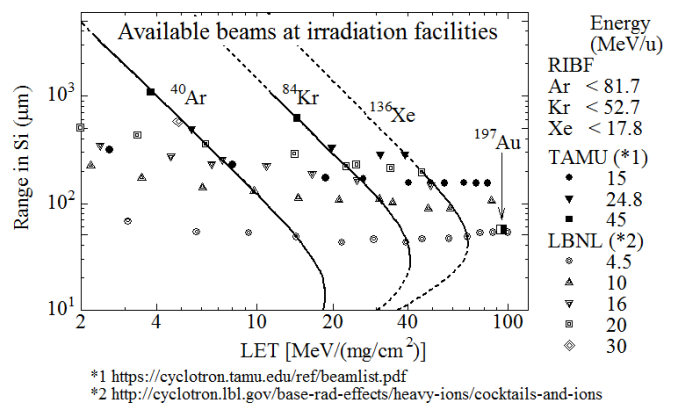


Fig. 1. LET and ion range relation of heavy ions in silicon at the client's sample position. Thick lines show the available range at RIBF.

Fig. 2 shows the beamline. At about 4 m upstream of the irradiation place, the beam is deflected by two wobbler magnets at 60-Hz frequency vertically and horizontally so that its beam-spot center traces a circle. Then, the beam passes through a Au scatterer foil where multiple scattering diffuses the beam spot to form a uniform dose distribution at the irradiation place.

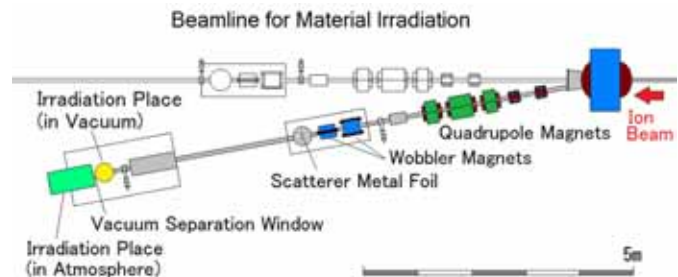


Fig. 2. Setup of the beamline for material irradiations.

Manuscript received July 9, 2018.

T. Kambara is with RIKEN Nishina Center, Wako, Saitama 351-0198 Japan (telephone: +81-48-467-9507, e-mail: kambara@ribf.riken.jp).

A. Yoshida is with RIKEN Nishina Center, Wako, Saitama 351-0198 Japan (telephone: +81-48-467-9423, e-mail: ayoshida@ribf.riken.jp)

Fig. 3 shows the irradiation place in the atmosphere at the end of the beamline. The beam passes through a vacuum-separation polyimide (Kapton) window with a diameter of 6 cm and thickness of 75 μm . A transmission-type ionization chamber (IC1) and a plastic scintillator behind the window measure the beam flux. A 5-cm diameter window of the IC1 determines the beam size downstream. An energy degrader has eleven Al foils with the thicknesses ranging from 5.5 to 2000 μm and any combination of the foils can be inserted to the beam by a remote-control pneumatic system so that the LET can be set almost continuously. Solid curves in Fig. 1 show the available LET and ion range of the Ar and Kr ions in silicon at the clients' sample position. The LET of Ar ions on a silicon surface is selectable between 2.2 and 18.7 MeV/(mg/cm²) and that of Kr ions between 11.7 and 41 MeV/(mg/cm²).

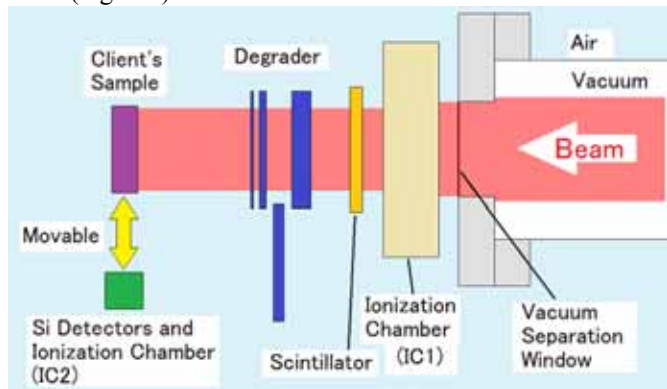


Fig. 3. Schematic diagram of the irradiation place at the end of the beamline where the beam is extracted to the atmosphere.

III. BEAM CHARACTERISTICS MEASUREMENTS

The characteristics of the beam are measured before each beam time for the clients. At the client's sample irradiation place, a shallow-type ionization chamber (IC2: 14-mm diameter, 2-mm thick) and two sets of $\Delta E+E$ Si-detector stacks are mounted on a motor-driven linear slider.

The IC2 output current is measured at different degrader thickness and the dependence is fitted by calculations of SRIM-2013 [2]. An example for a Kr beam is shown in Fig. 4. Fig. 4(a) shows the IC2 current as a function of the degrader thickness up to 900 μm . It also shows the best-fit result of SRIM-2013 calculation for the energy loss of the ions in IC2 and the measurements are normalized to the calculation. Fig. 4(b) shows the Bragg-peak region of Fig. 4(a) with the best-fit SRIM-2013 calculation and those with Al thickness altered by $\pm 10 \mu\text{m}$. It shows that with the best-fit result to the Bragg-peak measurement, the beam energy at the sample is determined within $\pm 5 \mu\text{m}$ accuracy of the range in Al. The actual degrader thicknesses for the LET desired by the clients are calculated with the SRIM-2013 code.

The Si detectors are used to measure the energy spectrum of the beam and to scan the beam for the beam-flux distribution. The measured beam-energy distribution is converted to LET distribution at different degrader thicknesses. The width of the LET obtained for Kr beam is

about 0.8 % FWHM of the mean LET at 12 MeV/(mg/cm²) and 5.6 % FWHM at 37 MeV/(mg/cm²). According to the beam scanning, the flux is uniform within 1.8 % over a diameter of about 35 mm. Another measurement with a GAFCHROMIC-film irradiation shows that the local deviation of the dose is within $\pm 5\%$.

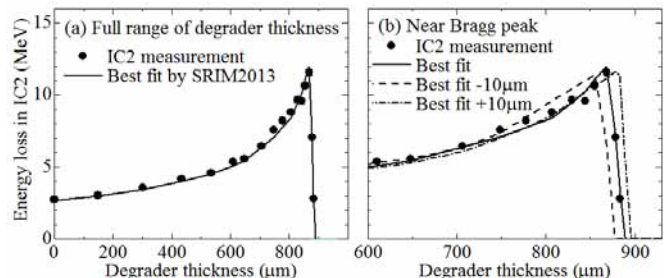


Fig. 4. Dependence of the ionization chamber IC2 output current on the degrader thickness. Dots are measured values fitted by SRIM calculations

Clients can select a beam flux between 10 and 10^7 ions/cm²/s. The flux is continuously monitored during irradiation. The scintillator is used for the flux measurements below 7×10^4 ions/cm²/s, and IC1 is used above it. The IC1 output current is calibrated by the ion count rate of the scintillator.

During an irradiation beam time, the beam flux and LET are controlled by the clients from outside of the radiation controlled area via LAN

IV. RADIOCHEMICAL ANALYSES OF IMPURITY NUCLIDES IN THE BEAM

The high-energy beam from the RRC passes through the window, the beam-flux detectors, the energy degrader and the atmosphere before reaching the client's sample. Nuclear reactions in these upstream materials convert a part of the beam nuclei to different nuclides. These nuclides may contaminate the beam and affect the LET distribution when they reach the client's sample.

We have studied the beam contamination employing a radiochemical method, where the primary Kr beam and impurity beams (secondary beams) were stopped in samples and the amount of radionuclides in them were measured by gamma-ray analyses. As this measurement is very sensitive, we can identify the radionuclides and obtain the absolute value of those production probabilities. Moreover, this measurement is insensitive to stable nuclides including the primary Kr ions and we can analyze very small amount of impurity radionuclides without being disturbed by background from the primary beam. However, this measurement is applicable only to radionuclides that have proper lifetimes and emit gamma-rays with proper energies. So, we compared the measurement results with an ion-transport simulation to evaluate its validity and discuss the impurity-beam as a whole on the basis of the simulation.

We irradiated test samples with an ⁸⁴Kr beam in the same condition as the client's irradiations. A 70-MeV/u ⁸⁴Kr beam from the RRC passed through a 50- μm -thick Au-foil scatterer, the 75- μm -thick Kapton window, a 15- μm -thick Al foil in the

IC1, 0.1-mm thick plastic scintillator, mylar foils of the detectors with the total thickness of 72- μm , the degrader with a 586- μm -thick Al and about 305-mm thick atmosphere, and impinging a test sample of Si wafer (100-mm diameter and 0.5-mm thick) or acrylic plate (75 mm \times 80 mm, 1-mm thick). The test sample of Si was used to simulate the client's sample of semiconductor devices and acrylic resin to distinguish the beam-impurity nuclides from the reaction products in the sample. The number of the ions was about 4.5×10^{10} for the Si wafers and 5.5×10^{10} for the acrylic plates during 10 minutes of irradiation. According to the SRIM calculation, the energy of the ^{84}Kr ions hitting the sample was 25 MeV/u which corresponded to the LET of about 19 MeV/(mg/cm²) in Si, and the ions stopped in the test samples.

We measured the gamma rays from the irradiated samples with Ge detectors; for the Si wafer, 9 times during the time span of 7 minutes to 91 days after the irradiation and for the acrylic plate, 9 times from 10 minutes to 106 days. We analyzed the observed gamma-ray peaks according to the transition energies, lifetimes and branching ratios, and identified about 61 nuclear species from ^{24}Na to ^{104}Ag in the Si wafer and 49 species from ^{24}Na to $^{93\text{m}}\text{Mo}$ in the acrylic plate, all with a half-life longer than 8 min. Then we extrapolated the decay curves of the radioactivity to the end of the irradiation to obtain the production rates of the nuclides and deduced their production probabilities normalized to one incident ^{84}Kr ion.

Some of the obtained nuclide-production probabilities in the Si and acrylic plates are shown in Fig. 5.

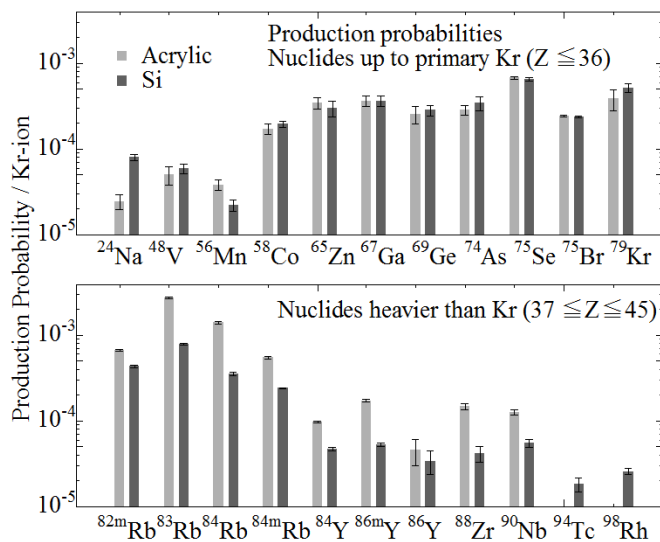


Fig. 5. Production probabilities of nuclides from ^{24}Na to ^{98}Rh obtained by the radiochemical analyses are compared between the test samples of Si wafer and acrylic plates.

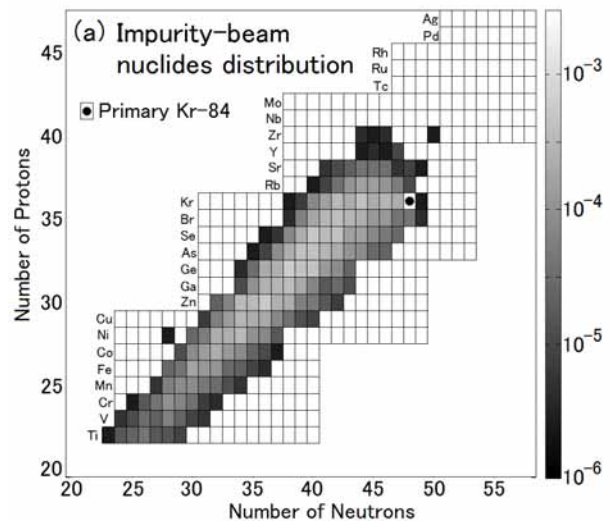
Comparing the probabilities between the Si and acrylic, we can group the nuclides by the atomic number Z . The probabilities for the nuclides up to the primary Kr ($Z \leq 36$) are very similar between the two materials except for a few small- Z nuclides, whereas the probabilities for $37 \leq Z \leq 42$ are higher in the acrylic than the Si and nuclides with $Z > 42$

are found only in the Si. It indicates that the low- Z nuclides consist mainly of nuclides produced in the upstream materials, those with $Z > 42$ are only produced by nuclear reactions in the Si sample, and those with $37 \leq Z \leq 42$ are produced by the both processes.

V. SIMULATION OF IMPURITY-NUCLIDES PRODUCTION

We simulated the production and transport of the nuclides in the irradiations with Particle and Heavy Ion Transport code System (PHITS) [3] which traced each resultant nucleus from its production to stopping. First, we assumed the same setup as the test-sample irradiations with the degrader thickness of 586 μm , calculated the probabilities that reaction-product nuclides are found in the sample and compared the results with the gamma-ray measurements.

PHITS predicts that the impurity beam consists mainly of nuclides with $20 < Z \leq 40$, which are produced from the primary Kr ions by high-velocity collisions with static nuclei. It also predicts that the nuclear reactions in the sample produce nuclides with Z up to 47. The results for a Si-wafer sample are shown in Fig. 6 where (a) is the probabilities for the impurity-beam nuclides produced in the upstream material and stopped in the sample, (b) is those for the nuclides produced by nuclear reactions in the sample and (c) is a sum of them. Fig. 6(c) also shows the results of the radiochemical analyses in circles. The overall features of the measurements look well reproduced by PHITS. It validates the use of PHITS to simulate our beam and irradiation.



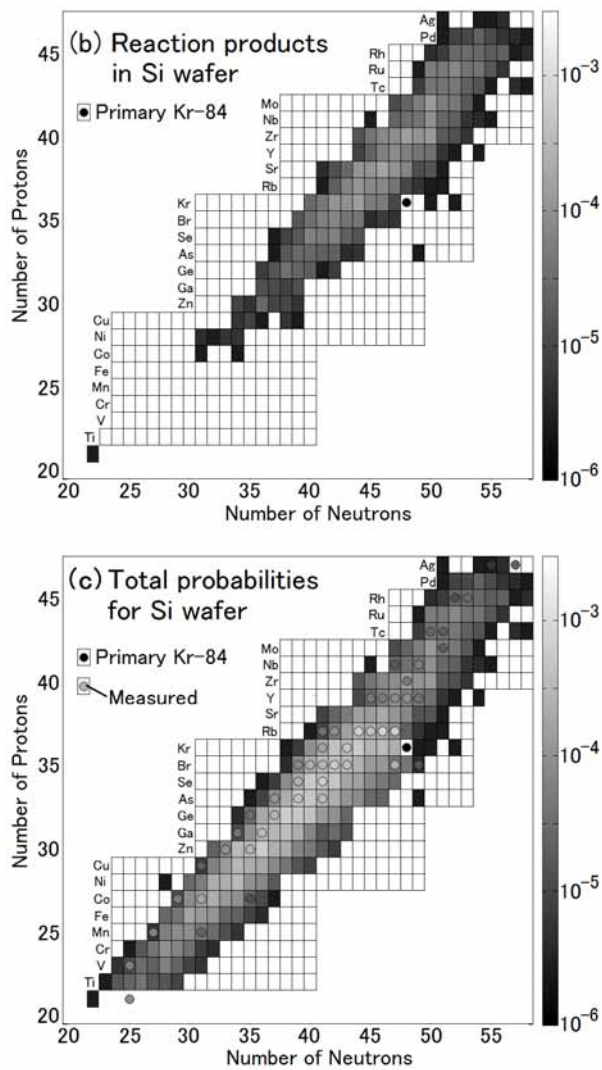


Fig. 6. PHITS results for probabilities of nuclides stopped in the Si-wafer sample when the degrader is 586- μm thick. Z is the atomic number and N is the number of neutrons of the nuclide and the probability is shown in the box by gray scale. (a) is for the impurity-beam nuclides, (b) is for the nuclides produced by the reactions in the sample and (c) is the sum of the two compared with the radiochemical measurements shown in the circles.

We now concentrate on the impurity beam such as shown in Fig. 6(a). We calculated the energy and LET distribution of nuclides of Z between 22 and 45 (from Ti to Rh) in the primary and impurity beam after passing the degrader with different thicknesses of 0, 300, 586, and 837 μm . Fig. 7 shows the energy distribution and Fig. 8 the LET distribution in Si where (a) of each figure is for the nuclides up to the primary Kr ions ($Z \leq 36$) and (b) for heavier nuclides ($Z > 36$). Each peak in Fig. 7a and Fig. 8a correspond to the primary Kr beam.

The energy of the primary Kr ions in Fig. 7(a) decreases at increasing intervals as the degrader thickness increases. Each of the energy distribution has a continuum below the peak, which corresponds to the impurity beam. When impurity-beam nuclides pass through materials, they lose energy quicker, and reach the Bragg peak and stop earlier, than the primary Kr ions. The heavier nuclides in Fig. 7(b) have lower

energies than the primary Kr beam and their intensity increases up to the degrader thickness of 586 μm . At degrader thickness of 837 μm , the total intensity of the impurity beam decreases but a significant part of it is slow and heavy nuclides.

Without degrader, a small fraction of the impurity beam have LET higher than that of the primary Kr ions, as shown in Fig. 8. When the degrader thickness increases, the energy distribution of the impurity beam shifts to lower energy and more of the impurity beam have LET higher than that of the primary Kr ions. At the thickness of 586 μm , the impurity-beam energy distributes between zero and the primary Kr peak, and the LET of most of the impurity beam exceeds that of the primary Kr ions. At the thickness of 837 μm where the primary Kr ions is close to the Bragg peak, most of the impurity beam is stopped before the sample and the amount of the impurity beam is small. However, the slow and high- Z nuclides shown in Fig. 7(b) give rise to LET as high as 50 MeVcm^2/mg as shown in Fig. 8(b). Probably, these very high-LET impurity nuclides originate in fusion-like reactions in the degrader. Similar reactions may produce ^{94}Tc and ^{98}Rh in Si as shown in Fig. 5.

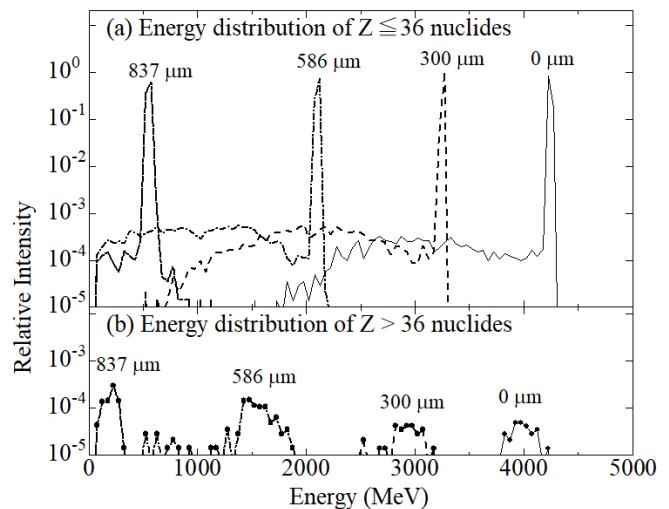


Fig. 7. PHITS results for energy distributions of the impurity-beam nuclides for degrader thicknesses of 0, 300, 586 and 837 μm . (a) is for the nuclides with $Z \leq 36$ and (b) for $Z > 36$.

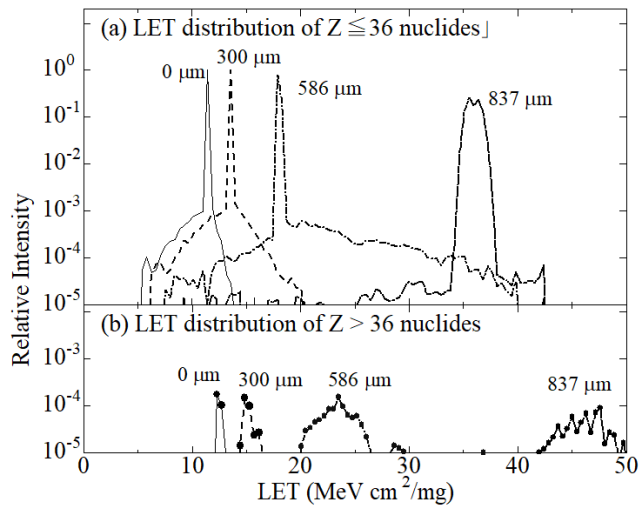


Fig. 8. PHITS results for LET distributions of the impurity-beam nuclides for degrader thicknesses of 0, 300, 586 and 837 μm . (a) is for the nuclides with $Z \leq 36$ and (b) for $Z > 36$.

The number of impurity nuclides which have higher LET than the primary ^{84}Kr ions is added up and the ratio of the sum to the number of the primary ^{84}Kr is plotted in Fig. 9 as a function of the degrader thickness. This high-LET impurity ratio has a maximum value of about 1.2 % at about 600 μm of the degrader thickness where the degrader is thick enough to produce and decelerate the impurity beams but the LET of the ^{84}Kr ions is still low.

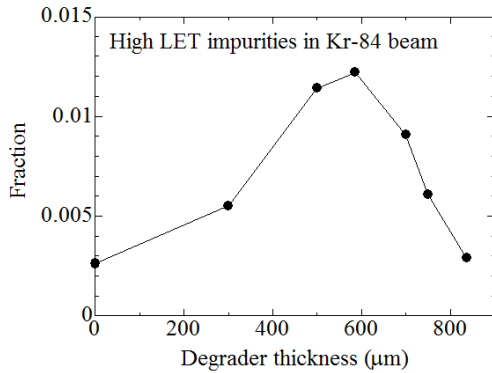


Fig. 9. The calculated ratio of the high-LET impurity nuclides in a Kr beam at the entrance of the client's sample is shown as a function of the degrader thickness.

VI. SUMMARY

The material irradiation facility of RIKEN RI Beam Factory is described. Semiconductor companies use Kr and Ar beams for SEE simulation with a uniform dose distribution and the LET selectable from 2.2 to 41 $\text{MeV}/(\text{mg}/\text{cm}^2)$. Samples can be irradiated in air and the clients can control the LET and beam flux from outside of the radiation-controlled area.

Production probabilities of impurity-beam RI nuclides were measured by radiochemical analyses of irradiated test samples. Heavy-ion transport simulations reproduced the overall features of the measured probabilities, and show that

high-LET impurity nuclides in the beam account for about 1 % of the Kr-beam at maximum.

VII. ACKNOWLEDGMENT

The authors are grateful to RNC's Nuclear Chemistry Research Team for providing their Ge detectors for the gamma-ray measurements. This experiment was performed at RI Beam Factory operated by RIKEN Nishina Center and CNS, University of Tokyo.

VIII. REFERENCES

- [1] H. En'yo, "A dream come true: our 80-plus-year history with nine cyclotrons at RIKEN," *Nuclear Physics News*, vol. 25, no. 3, pp. 5-12, Sep. 2015.
- [2] J. F. Ziegler, "The Stopping and Range of Ions in Matter", <http://www.srim.org/>, 2013.
- [3] T. Sato, Y. Iwamoto, S. Hashimoto, T. Ogawa, T. Furuta, S. Abe, T. Kai, P.-E. Tsai, N. Matsuda, H. Iwase, N. Shigyo, L. Sihver and K. Niita, "Features of particle and heavy ion transport code system (PHITS) version 3.02," *J. Nucl. Sci. Technol.* vol. 55, pp. 684-690, Jan. 2018.